IEEE Access
Multidisciplinary | Rapid Review | Open Access Journal

IEEE POWER & ENERGY SOCIETY SECTION

Received April 30, 2022, accepted May 13, 2022, date of publication May 17, 2022, date of current version May 23, 2022.

Digital Object Identifier 10.1109/ACCESS.2022.3175891

A Novel Electromagnetic Transient Simulation Method of Large-Scale AC Power System With High Penetrations of DFIG-Based Wind Farms

YIFENG DONG[1], JIANBO GUO[2], (Senior Member, IEEE), SHIHONG MIAO[1], (Member, IEEE), JUNXIAN HOU[3], JI HAN[1], (Student Member, IEEE), SHICONG MA[2], AND TIEZHU WANG[2]

[1]School of Electrical and Electronic Engineering, Huazhong University of Science and Technology, Wuhan 430074, China
[2]China Electric Power Research Institute, Beijing 100192, China
[3]Wanliyang Energy Technology Company Ltd., Hangzhou 310059, China

Corresponding author: Yifeng Dong (yifengdong@163.com)

This work was supported in part by the National Key Research and Development Program of China under Grant 2016YFB0900600.

ABSTRACT With the ever-expanding deployment of renewable energy sources (RESs), the short-time transients have more significant impacts on shaping the characteristics of large power grids. However, the electro-mechanic transient simulation cannot reflect the short-time transients, while the current electromagnetic transient simulation cannot tackle large power systems due to the huge computational burden. This paper presents a novel simplified electromagnetic transient simulation method for large-scale power systems with high penetrations of doubly fed induction generator (DFIG)-based wind farms. Firstly, a DFIG-based wind generator (WG) model is built to simplify the detailed switching process of power electronic devices as well as reproduce external characteristics of the power system. Secondly, an initialization technique is further adopted using the power flow results, aiming to avoid the long and unnecessary computation process for starting the simulation with traditional methods. Finally, a simulation tool is developed based on the proposed method, and a real power system with 9889 buses and 898 wind farms is simulated. Results show that the simulation can start smoothly with good accuracy. Therefore, the proposed method can be employed in electromagnetic transient simulation of large-scale AC power systems with high penetrations of RESs.

INDEX TERMS Electromagnetic transient simulation, DFIG-based wind farm, initialization, and electro-mechanic transient simulation.

I. INTRODUCTION

Power systems are one of the largest manmade complex systems and support most activities in modern society. The simulation techniques are compulsory for analyzing today's power systems as direct analytical methods are nearly infeasible. For conventional power systems dominated by synchronous machines, electro-mechanic transient simulations have been used.

With the economical constraints, intermittent renewable energy sources (RESs), such as wind power and photovoltaic power, have been widely deployed in the power system. Differing from traditional power plants that use synchronous generators to interact with the grid, RESs use power electronic converters [1], [2]. As a result, the specific dynamics of RESs and their interactions with the AC power grid are playing more important roles in shaping the characteristics of large-scale power grids [3], [4].

Differing from the traditional AC devices, power electronics converters have more complicated control strategies that can switch quickly. Besides, they have nearly zero inertia that induces faster oscillations in the face of the same disturbance and much lower overload capacity that triggers protection actions in a short time. For example, when a fault occurs in the power system, the converters can switch to the low voltage ride-through (LVRT), thus having a significant influence on the voltage and frequency of the power system [5]–[7]. In some special cases, the interaction between the convertor and AC system may cause low-frequency or high-frequency oscillations [8], [9]. Usually, the above new dynamical characteristics cannot be described with electro-mechanic transient simulation, as it is not suitable for the simulation

The associate editor coordinating the review of this manuscript and approving it for publication was Feng Wu.

of short-time transient processes. In particular, when large amounts of electronic converters are connected to the AC power system, it is difficult to simulate the system precisely because the short-time electromagnetic transient process may influence the long-time electro-mechanic transient process of the whole power system.

Instead, electromagnetic transient simulation tools have been applied, such as PSCAD [10], RTLAB [11], etc. Currently, the electromagnetic transient simulation [12] can model power electronics devices with high precision and simulate the short-time transient processes. However, the detailed modeling and the small time-step greatly increase the computation burden and heavily limit the simulation range of the power system. Therefore, the current electromagnetic transient simulation is usually applied to the device-level simulation while cannot simulate the large-scale power system with a longer time range [13].

To make the electromagnetic transient simulation method be able to simulate the electro-mechanic processes of large-scale power systems, a series of problems should be solved, such as the simplified modeling, the efficient initialization, etc. In the conventional modeling of wind power plants in electromagnetic transient simulation [14]–[21], the switching processes of power electronics circuits are described in detail, which significantly increases the computation costs as well as reduces the efficiency. Meanwhile, these switching processes have little effect on the external characteristics of the converter to the AC power grid. So it is feasible to simplify the switching processes in the modeling to balance efficiency and accuracy. The initialization is another important issue. The initialization process in the conventional electromagnetic transient simulation usually starts from zero. When applied to the large-scale power system, this kind of initialization is laborious and time-consuming, and even can fail. By referring to the initialization technique applied in electro-mechanic transient simulation that is extremely fast and steady, the result of power flow can be used in the initialization of the electromagnetic transient simulation.

The paper proposes a novel electromagnetic transient simulation method for large-scale AC power systems with high penetrations of doubly fed induction generator (DFIG)-based wind farms. Specifically, the modeling of DFIG-based wind generator (WG) is presented in Section II; the considerations of its interfaces to the AC power grid are introduced in Section III; the initialization technique is given in Section IV; the transient simulation process is presented in Section V; the simulation results are proposed in Section VI. Results show that the proposed method can seek a balance between computational cost and simulation accuracy by simplifying the switching process and initializing based on the result of power flow.

II. MODELING OF DFIG-BASED WIND GENERATORS

Modeling of DFIG-based WG is the basis for the electromagnetic transient simulation of large-scale power systems with high penetrations of DFIG-based wind farms.

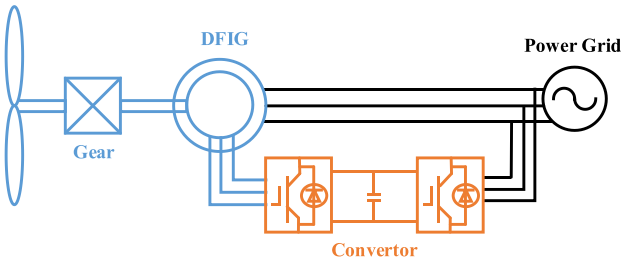

FIGURE 1. Structure diagram of DFIG-based WG.

To achieve a good balance between efficiency and accuracy, the model considers the application purpose and limitations of large-scale power system simulation.

A. BASIC MODELING PHILOSOPHY

The model should be suitable for the electromagnetic transient simulation of a large-scale power system. How detailed the model needs to be built is determined by the application purpose and scenario. It needs to select a proper model to balance the efficiency and accuracy.

The usual model of electromagnetic transient simulation deals with the electronic switching process in detail. It can be used to simulate the internal and external transient process of microsecond-level. Therefore, it is suitable for detailed simulation of equipment. However, it needs heavy computation.

In the electromagnetic transient simulation of a large-scale AC power system with wind power, the external transient characteristic of wind power is the main consideration while the internal transient process can be simplified. Thus, the modeling ignores the electronic switching process of the wind power and the convertor can be equivalent to a voltage source that considers the limit of modulation and the relationship between AC and DC voltage. As the convertor of DFIG-based WG is composed of full control devices and has an ideal external characteristic, the equivalent of the convertor is suitable and the error is small. Moreover, the simplification of the electromagnetic transient model greatly reduces the computation.

Although the simplified electromagnetic transient model is similar to the electromechanical transient model, compared with the electro-mechanic transient model, it adds some quickly responsive parts and the ones that cannot be simulated by the electro-mechanic transient model, which makes short-time transient simulation more accurate.

In brief, the simplified model is between the detailed electromagnetic transient simulation model and electromechanical simulation model, which mainly models the external characteristics from microsecond-level to minute-level that have a significant impact on a power system.

B. MODEL STRUCTURE

The structure diagram of DFIG-based WG is shown in Figure 1. The stator of the generator is directly connected to the power grid, and the rotor is fed by self-commutated converters. The converters include the rotor side and grid side. The

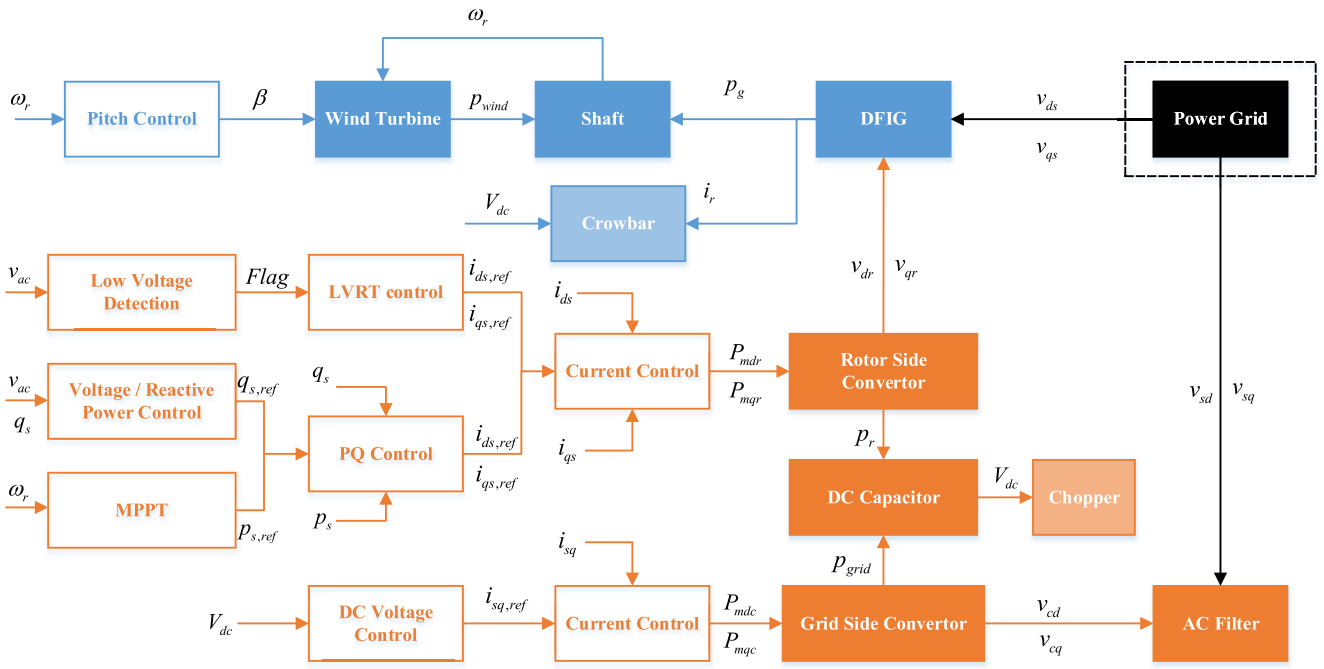

FIGURE 2. Model structure of DFIG-based WG.

rotor side converter controls the rotor voltage in magnitude and phase angle. Therefore, it can be used for active and reactive power control. The control system of the convertor is the most important part of the model.

The electromagnetic transient model includes the physical devices, control system, and protection. The model structure is shown in Figure 2.

The direction of stator flux is selected as the d-axis for DFIG and rotor side converter. The direction of AC voltage is selected as the d-axis for the grid-side convertor. The q-axis is ahead 90 degrees of the d-axis.

The model includes the following several parts:

1) The physical parts include a wind turbine, shaft, DFIG, rotor side convertor, DC capacitor, grid side convertor, and AC filter. The model of the converter should be simplified and mainly considers the external characteristic. AC filter can be equivalent to an inductance.

2) The control system models include pitch angle control, rotor side convertor control, and grid side converter control. The rotor side converter controls the rotor voltage and further controls the active and reactive power. The grid side converter keeps the DC voltage constant. The control of the rotor side converter has the greatest influence on the transient process of the power system, especially in the low voltage ride-though (LVRT) status.

3) The protections include crowbar and chopper to limit the DC voltage and rotor current.

The above models have been studied and applied before. However, when used in the electromagnetic transient simulation of AC power systems with large-scale DFIG-based wind farms, it is necessary to select suitable models. The paper mainly elaborates on the convertor model and the control model of the rotor side converter, as is shown in Figure2.

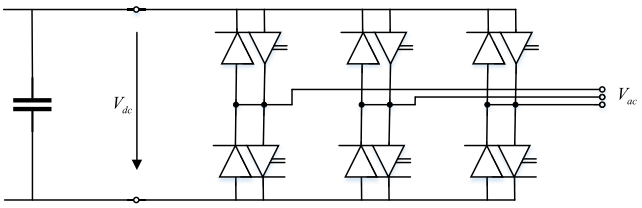

FIGURE 3. Basic structure of Convertor.

C. CONVERTOR MODEL

The basic structure of the converter is shown in Figure 3.

Converter models usually include detailed model, average-value model, etc. The simplified model in this paper is based on the average-value model. According to the average-value model of converter, the converter can be equivalent to three controlled voltage sources (v_a, v_b, and v_c) on the AC side and a controlled current source on the DC side. As shown in Figure 4(a). Taking the two-level converter as an example, the equivalent controlled voltage source is as follows [32]:

$$\begin{cases} v_a = \frac{1}{2} V_{dc} * m_a \\ v_b = \frac{1}{2} V_{dc} * m_b \\ v_c = \frac{1}{2} V_{dc} * m_c \end{cases} \tag{1}$$

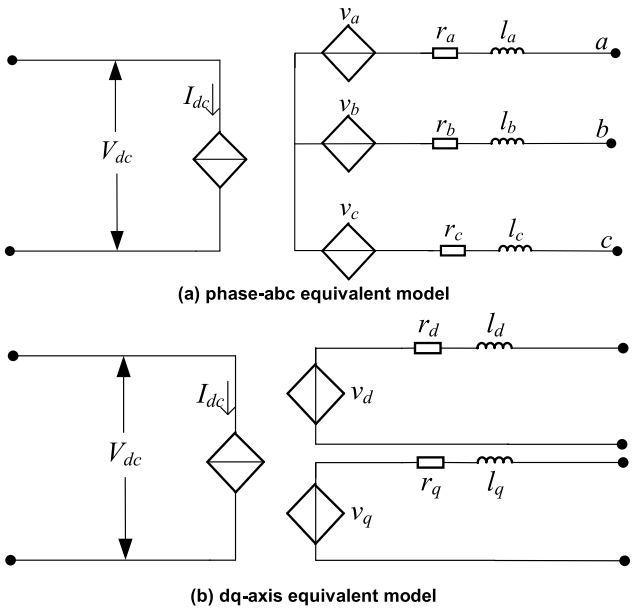

FIGURE 4. Equivalent model diagram of converter.

$$\begin{cases} m_a = P_{ma}\cos(\omega t + \delta) \\ m_b = P_{mb}\cos\left(\omega t + \delta - \dfrac{2\pi}{3}\right) \\ m_c = P_{mc}\cos\left(\omega t + \delta + \dfrac{2\pi}{3}\right) \end{cases} \tag{2}$$

where m_a, m_b, m_c are the modulation functions generated by the pulse width modulation (PWM) control system respectively; V_{dc} is the voltage of the DC capacitor; P_{ma}, P_{mb}, P_{mc} are the modulation ratios of phase a, b and c respectively, which are defined as the ratio of the maximum value of the modulating wave to the maximum value of the carrier wave. In a two-level converter, its value is the ratio between the maximum fundamental peak phase voltages to half of DC voltage.

The equivalent model in phase-*abc* can be converted into the equivalent model in *dq*-axis, as shown in Figure 4(b), in which the equivalent voltage source is:

$$\begin{cases} v_d = K_0 P_{md} V_{dc} \\ v_q = K_0 P_{mq} V_{dc} \end{cases} \tag{3}$$

where, v_d and v_q are d-axis voltage and q-axis voltage respectively; P_{md} and P_{mq} are the modulation ratio of d-axis and q-axis, corresponding to the output signal of "current control" module in Figure 2; K_0 is a constant related to the modulation mode. When sinusoidal pulse width modulation (SPWM) mode is adopted, $K_0 = 1/2$.

Based on the power balance between AC and DC sides, ignoring the loss of the converter, the controlled current source on DC side can be expressed as

$$I_{dc} = p_{ac}/V_{dc} \tag{4}$$

where, p_{ac} is the total active power on the AC side of the converter.

Equation (3) express the external characteristic. The AC voltage has a linear relationship with DC voltage when the modulation ratio is below 1.0. The model considers the fundamental frequency component, ignores the power loss and has ideal external characteristics. In terms of AC dynamic performance, the proposed model has satisfactory effect, and the simulation speed is fast [33]. Therefore, it is suitable for large power grid simulation.

D. CONTROL MODEL OF ROTOR SIDE CONVERTOR

The rotor side converter controls the rotor voltage and further controls the active and reactive power. The control of the rotor side has the greatest influence on the external characteristic of DFIG-based WG, especially LVRT control which must be modeled in the transient simulation.

The model of DFIG includes voltage equations and flux-linkage equations, the positive direction of stator and rotor current is selected to flow into the generator, the equations are listed as (5) and (6).

$$\begin{cases} v_{ds} = r_s i_{ds} + \dfrac{d\lambda_{ds}}{dt} - \omega_s \lambda_{qs} \\ v_{qs} = r_s i_{qs} + \dfrac{d\lambda_{qs}}{dt} + \omega_s \lambda_{ds} \\ v_{dr} = r_r i_{dr} + \dfrac{d\lambda_{dr}}{dt} - (\omega_s - \omega_r)\lambda_{qr} \\ v_{qr} = r_r i_{qr} + \dfrac{d\lambda_{qr}}{dt} + (\omega_s - \omega_r)\lambda_{dr} \end{cases} \tag{5}$$

$$\begin{cases} \lambda_{ds} = L_s i_{ds} + L_m i_{dr} \\ \lambda_{qs} = L_s i_{qs} + L_m i_{qr} \\ \lambda_{dr} = L_m i_{ds} + L_r i_{dr} \\ \lambda_{qr} = L_m i_{qs} + L_r i_{qr} \end{cases} \tag{6}$$

$$\begin{cases} L_s = l_s + l_m \\ L_m = l_m \\ L_r = l_r + l_m \end{cases} \tag{7}$$

where v_{ds} and v_{qs} are stator voltage; i_{ds} and i_{qs} are stator current; λ_{ds} and λ_{qs} are stator flux; v_{dr} and v_{qr} are rotor voltage; i_{dr} and i_{qr} are rotor current; λ_{dr} and λ_{qr} are rotor flux; the above variables are expressed by the *dq*-axis. r_s and l_s are stator resistance and stator inductance; r_r and l_r are rotor resistance and inductance; l_m is magnetic inductance; ω_s and ω_r are rotate speed of system and rotor; L_s, L_r and L_m are defined as self-inductance of the stator, self-inductance of the rotor and mutual inductance between stator and rotor respectively.

The active and reactive power can be expressed as

$$\begin{cases} p_s = v_{ds} i_{ds} + v_{qs} i_{qs} \\ q_s = v_{ds} i_{qs} - v_{qs} i_{ds} \end{cases} \tag{8}$$

where, p_s and q_s are stator active and reactive power.

The direction of stator flux is selected as d-axis, and the q-axis is ahead of d-axis for 90 degrees. Then, the stator flux of q-axis will be zero.

$$\lambda_{qs} = 0 \tag{9}$$

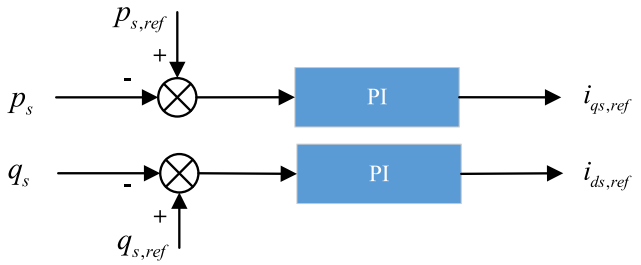

FIGURE 5. Schematic diagram of PQ control model.

According to the equation (5)-(9), the following equation can be derived:

$$v_{ds} = 0 \tag{10}$$

$$\begin{cases} p_s = v_{qs} i_{qs} \\ q_s = -v_{qs} i_{ds} \end{cases} \tag{11}$$

$$\begin{cases} i_{dr} = \dfrac{1}{L_m}\lambda_{ds} - \dfrac{L_s}{L_m} i_{ds} \\ i_{qr} = -\dfrac{L_s}{L_m} i_{qs} \end{cases} \tag{12}$$

$$\begin{cases} v_{dr} = r_r i_{dr} + \left[L_r - \dfrac{(L_m)^2}{L_s} \right] \dfrac{di_{dr}}{dt} + \Delta v_{dr} \\ v_{qr} = r_r i_{qr} + \left[L_r - \dfrac{(L_m)^2}{L_s} \right] \dfrac{di_{qr}}{dt} + \Delta v_{qr} \end{cases} \tag{13}$$

$$\begin{cases} \Delta v_{dr} = -(\omega_s - \omega_r) \left[L_r - \dfrac{(L_m)^2}{L_s} \right] i_{qr} \\ \Delta v_{qr} = (\omega_s - \omega_r) \dfrac{L_m}{L_s} \lambda_{ds} \\ \quad + (\omega_s - \omega_r) \left[L_r - \dfrac{(L_m)^2}{L_s} \right] i_{dr} \end{cases} \tag{14}$$

According to (11), the control of p_s and q_s can be realized by the control of i_{qs} and i_{ds} which is shown in Figure 5. It is corresponding to the "PQ control" of Figure 2.

Then, the rotor current is computed by equation (12) and the rotor voltage is controlled using equations (13) and (14), which are shown in Figure 6. It is corresponding to the "Current control" of Figure 2.

Figures 5 and 6 realize the normal control of the rotor side converter. When the AC voltage is below the limit, for example, 0.9 p.u., the LVRT control replaces the normal PQ control to control the active and reactive current. The general active and reactive power curve of LVRT is shown in Figure 7.

During LVRT, the active current may be kept at a fixed value, and the reactive current usually increases according to the AC voltage, as in (15).

$$i_{ds,ref} = k_q \left(v_{ref} - v_{ac} \right) \tag{15}$$

where v_{ref} is the voltage constant usually is 0.9 p.u., v_{ac} is the AC voltage, k_q is constant usually great than 1.5, $i_{ds,ref}$ is the reactive current. The reactive current is usually prior, and

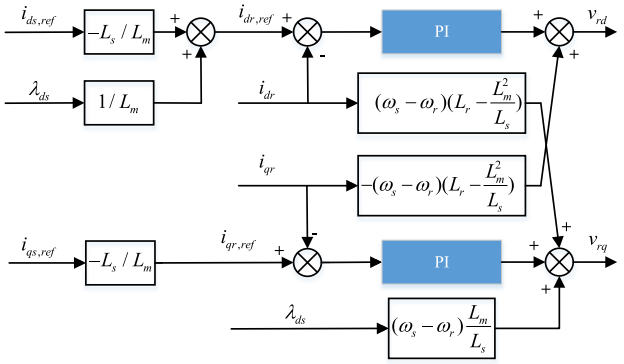

FIGURE 6. Schematic diagram of current control model.

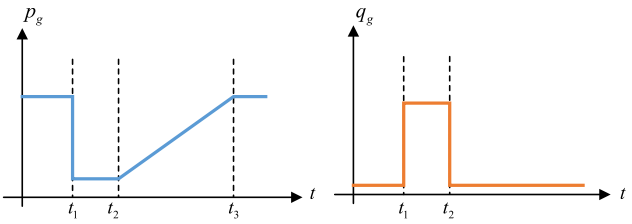

FIGURE 7. The general active and reactive power curve of LVRT.

the limit of active current is computed by equation (16).

$$i_{qs,lim} = \sqrt{i_{s,lim}^2 - i_{ds,ref}^2} \tag{16}$$

where $i_{s,lim}$ is the total current limit, $i_{qs,lim}$ is the active current limit. Because the reactive current is usually high, the active current is limited to a small value.

After the LVRT, reactive current returns to normal control, and active current increases at a certain rate until reaching the value of normal control.

III. INTERFACE WITH THE AC POWER GRID

The interface between the DFIG-based WG and the AC power system is an important part of the model. The DFIG-based WG can be equivalent to the parallel of conductance and current source. The stator of DFIG-based WG and the convertor of the grid side are connected to the power grid separately, so the interfaces need to be processed separately.

Based on the implicit trapezoidal integral method [22], [23], the equation (17) - (23) can be derived from (5) and (6).

$$\begin{cases} v_{ds} = R_{equ} i_{ds} + v_{dseq} \\ v_{qs} = R_{equ} i_{qs} + v_{qseq} \end{cases} \tag{17}$$

$$R_{seq} = r_s + \frac{2l_s}{\Delta t} + \frac{\frac{2l_m}{\Delta t}\left(r_r + \frac{2l_r}{\Delta t} \right)}{r_r + \frac{2l_r}{\Delta t} + \frac{2l_m}{\Delta t}} \tag{18}$$

$$\begin{cases} v_{dseq} = v_{dseq1} + v_{dseq,\Delta t} \\ v_{qseq} = v_{qseq1} + v_{qseq,\Delta t} \end{cases} \tag{19}$$

$$\begin{cases} v_{dseq1} = \gamma v_{dr} - \omega_s \lambda_{qs} + (\omega_s - \omega_r)\gamma \lambda_{qr} \\ v_{qseq1} = \gamma v_{qr} + \omega_s \lambda_{ds} - (\omega_s - \omega_r)\gamma \lambda_{dr} \end{cases} \tag{20}$$

$$\begin{cases} v_{dseq,\Delta t} = -\dfrac{2}{\Delta t}F_{ds,\Delta t} + \gamma\dfrac{2}{\Delta t}F_{dr,\Delta t} \\ v_{qseq,\Delta t} = -\dfrac{2}{\Delta t}F_{qs,\Delta t} + \gamma\dfrac{2}{\Delta t}F_{qr,\Delta t} \end{cases} \tag{21}$$

$$\begin{cases} F_{ds,\Delta t} = \lambda_{ds,\Delta t} + \dfrac{\Delta t}{2} \\ \left(v_{ds,\Delta t} - r_s i_{ds,\Delta t} + \omega_{s,\Delta t}\lambda_{qs,\Delta t}\right) \\ F_{qs,\Delta t} = \lambda_{qs,\Delta t} + \dfrac{\Delta t}{2} \\ \left(v_{qs,\Delta t} - r_s i_{qs,\Delta t} - \omega_{s,\Delta t}\lambda_{ds,\Delta t}\right) \\ F_{dr,\Delta t} = \lambda_{dr,\Delta t} + \dfrac{\Delta t}{2}\left[v_{dr,\Delta t} - r_r i_{dr,\Delta t}\right. \\ \left. + \left(\omega_{s,\Delta t} - \omega_{r,\Delta t}\right)\lambda_{qr,\Delta t}\right] \\ F_{qr,\Delta t} = \lambda_{qr,\Delta t} + \dfrac{\Delta t}{2}\left[v_{qr,\Delta t} - r_r i_{qr,\Delta t}\right. \\ \left. - \left(\omega_{s,\Delta t} - \omega_{r,\Delta t}\right)\lambda_{dr,\Delta t}\right] \end{cases} \tag{22}$$

$$\gamma = \frac{\frac{2l_m}{\Delta t}}{r_r + \frac{2l_r}{\Delta t} + \frac{2l_m}{\Delta t}} \tag{23}$$

where Δt is the time-step; R_{seq} is equivalent resistor; v_{dseq} and v_{qseq} are two parts of the equivalent voltage source; v_{dseq1} and v_{dseq1} are the first parts and computed by the value of current time-step; $v_{dseq,\Delta t}$ and $v_{qseq,\Delta t}$ are the second parts and computed by the value of the previous time-step.

Equation (17) is converted to three phases, then changed to the parallel of conductance and current source, as in (24) - (26).

$$\begin{bmatrix} i_{as} \\ i_{bs} \\ i_{cs} \end{bmatrix} = G_{seq}\begin{bmatrix} v_{as} \\ v_{bs} \\ v_{cs} \end{bmatrix} + I_{seq} \tag{24}$$

$$G_{seq} = \begin{bmatrix} \dfrac{1}{R_{seq}} & 0 & 0 \\ 0 & \dfrac{1}{R_{seq}} & 0 \\ 0 & 0 & \dfrac{1}{R_{seq}} \end{bmatrix} \tag{25}$$

$$I_{seq} = -\frac{1}{R_{seq}}\begin{bmatrix} v_{dseq}cos\theta - v_{qseq}sin\theta \\ v_{dseq}cos\left(\theta - \dfrac{2\pi}{3}\right) \\ -v_{qseq}sin\left(\theta - \dfrac{2\pi}{3}\right) \\ v_{dseq}cos\left(\theta + \dfrac{2\pi}{3}\right) \\ -v_{qseq}sin\left(\theta + \dfrac{2\pi}{3}\right) \end{bmatrix} \tag{26}$$

where θ is delta angle of d-axis to x-axis; a, b and c denote three phases;I_{seq} is the equivalent current source; G_{seq} is the equivalent conductance matrix.

The AC filter connected with the power grid and grid-side convertor is usually modeled as a reactance. The relationship between voltage and current is:

$$\begin{cases} \Delta v_a = L\dfrac{di_a}{dt} \\ \Delta v_b = L\dfrac{di_b}{dt} \\ \Delta v_c = L\dfrac{di_c}{dt} \end{cases} \tag{27}$$

where L is the reactance; Δv_a, Δv_b, and Δv_c are voltage difference; i_a, i_b, and i_b are current.

Based on the implicit trapezoidal integral method, equation (28) - (30) can be derived from (27).

$$\begin{bmatrix} i_a \\ i_b \\ i_c \end{bmatrix} = G_{geq}\begin{bmatrix} \Delta v_a \\ \Delta v_b \\ \Delta v_c \end{bmatrix} + I_{geq,\Delta t} \tag{28}$$

$$G_{geq} = \begin{bmatrix} \dfrac{\Delta t}{2L} & 0 & 0 \\ 0 & \dfrac{\Delta t}{2L} & 0 \\ 0 & 0 & \dfrac{\Delta t}{2L} \end{bmatrix} \tag{29}$$

$$I_{geq,\Delta t} = \frac{\Delta t}{2L}\begin{bmatrix} \Delta v_{a,\Delta t} \\ \Delta v_{b,\Delta t} \\ \Delta v_{c,\Delta t} \end{bmatrix} + \begin{bmatrix} i_{a,\Delta t} \\ i_{b,\Delta t} \\ i_{c,\Delta t} \end{bmatrix} \tag{30}$$

where G_{geq} is equivalent conductance matrix, $I_{geq,\Delta t}$ is the equivalent current source computed by the value of the previous step.

The total equivalent conductance matrix and current source are

$$G_{eq} = G_{seq} + G_{geq} \tag{31}$$

$$I_{eq} = I_{seq} + I_{geq,\Delta t} \tag{32}$$

where G_{eq} is the total equivalent conductance matrix which is added to the conductance matrix of the power grid; I_{eq} is the total equivalent current resource which is added to the injection current vector of the power grid.

IV. INITIALIZATION TECHNIQUE

At the beginning of the transient simulation, the initial state must be established, then the simulation can be carried out with this initial state.

When the electromagnetic transient simulation is applied to the large-scale AC power system with high penetrations of wind power, there exist many variables and complex relationships among the variables. It is almost impossible to use the common zero-start method to initialize all the variables. Therefore, it is necessary to study a new method.

The electromechanical transient simulation of large-scale power systems is widely used. Before the simulation, power flow is computed and a system state is obtained. Then the initialization values of all variables are computed based on the result of power flow. If this initialization method is applied to electromagnetic transient simulation, it can effectively solve the difficulty of initialization from zero. However, there are two problems to be solved.

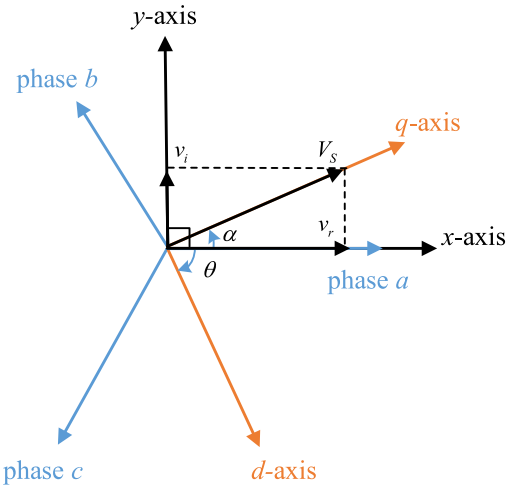

FIGURE 8. The relationship of three-phase abc, xy-axis, and dq-axis.

The first problem is to build the relationship between the instantaneous value, RMS value, and *dq*-axis value. The voltage of power flow is expressed as an RMS value including the real part and imaginary part. The voltage and current of electromagnetic transient simulation are expressed as the instantaneous values of a, b, and c phases. The data of the DFIG-based WG model is expressed as the value of the *dq*-axis.

As shown in Figure 8, there are three types of axes including *abc*, *xy*, *dq*, which are corresponding to the instantaneous value, RMS value, and *dq*-axis value.

The bus voltage $\dot{v}_s$ can be obtained from the result of power flow including the real and imaginary parts, as in (33).

$$\dot{v}_s = v_r + jv_i \tag{33}$$

where v_r and v_i are the real and imaginary parts of bus voltage.

The *y*-axis is 90 degrees ahead of the *x*-axis, and corresponds to the real and imaginary parts of the bus voltage. The difference among the *a*, *b*, and *c* phases is 120 degrees, and *a* phase corresponds with *x*-axis. The *q*-axis is 90 degrees ahead of *d*-axis, and *q*-axis corresponds with the direction of bus voltage.

The angle of $\dot{v}_s$ to the *x*-axis is computed by:

$$\alpha = \tan^{-1}\frac{v_i}{v_r} \tag{34}$$

The angle of *d*-axis to *x*-axis is computed by:

$$\theta = \alpha - \frac{\pi}{2} \tag{35}$$

The transformation matrices from three-phase *abc* to *dq0*-axis and from *dq0*-axis to three-phase *abc* are as in (36) and (37). Usually, the DFIG modelling and control use the Park transformation in the *dq*-axis, and the transformation matrices are the P with its third row removed and the P^{-1} with its third column removed respectively.

$$P = \frac{2}{3}\begin{bmatrix} \cos\theta & \cos\left(\theta - \frac{2\pi}{3}\right) & \cos\left(\theta + \frac{2\pi}{3}\right) \\ -\sin\theta & -\sin\left(\theta - \frac{2\pi}{3}\right) & -sin\left(\theta + \frac{2\pi}{3}\right) \\ 1/2 & 1/2 & 1/2 \end{bmatrix} \tag{36}$$

$$P^{-1} = \begin{bmatrix} cos\theta & -sin\theta & 1 \\ \cos(\theta - \frac{2\pi}{3}) & -sin(\theta - \frac{2\pi}{3}) & 1 \\ cos(\theta + \frac{2\pi}{3}) & -sin(\theta + \frac{2\pi}{3}) & 1 \end{bmatrix} \tag{37}$$

Another problem is the selection of reference values for per unit computation. The reference values of voltage, current, and frequency are usually the peak value of rated phase voltage, the peak value of rated line current, and rated frequency of the power system respectively. Other reference values are computed based on these three values.

Then, the initialization can be executed. The initialization includes 3 steps, as follows:

1) Compute voltage of *dq*-axis and three-phase *abc* component based on the value of power flow

The bus voltage of power flow is expressed as (33). The *dq*-axis and three-phase *abc* component can be computed by equations (38) and (39).

$$\begin{cases} v_d = 0 \\ v_q = \sqrt{v_r^2 + v_i^2} \end{cases} \tag{38}$$

$$\begin{cases} v_a = -v_q \sin\theta \\ v_b = -v_q \sin\left(\theta - \frac{2\pi}{3}\right) \\ v_c = -v_q \sin\left(\theta + \frac{2\pi}{3}\right) \end{cases} \tag{39}$$

where, v_d and v_q are the values of *d*-axis and *q*-axis; v_a, v_b and v_c are the values of phases *a*, *b*, and *c*.

2) Compute the initial value of all variables

As shown in Figure 2, the total model includes many parts, and all the variables of every part should be computed based on the initial voltage, initial power, and some other rated value. The initialization is complex and requires heavy computation. Take the initialization of the generator as an example.

The initial active and reactive power can be obtained from the result of power flow. The active power of stator and rotor is distributed basically according to the slip of DFIG. The reactive power of stator is the initial value of generator because the reactive power of the grid-side convertor is usually zero. The initial value of stator power can be computed by equation (40).

$$\begin{cases} p_s = p_g / (1 - s) \\ q_s = q_g \end{cases} \tag{40}$$

where p_g and q_g are active and reactive power of DFIG from the result of power flow; p_s and q_s are the active and reactive power of stator; s is slip of DFIG.

All the variables of the generator can be computed as in (41) - (46).

$$\begin{cases} v_{ds} = v_d \\ v_{qs} = v_q \end{cases} \tag{41}$$

$$\begin{cases} i_{ds} = \dfrac{p_s v_{ds} + q_s v_{qs}}{\sqrt{v_{ds}^2 + v_{qs}^2}} \\ i_{qs} = \dfrac{p_g v_{qs} - q_g v_{ds}}{\sqrt{v_{ds}^2 + v_{qs}^2}} \end{cases} \tag{42}$$

$$\begin{cases} \lambda_{ds} = v_{qs} - r_s i_{qs} \\ \lambda_{qs} = -v_{ds} + r_s i_{ds} \end{cases} \tag{43}$$

$$\begin{cases} i_{dr} = \dfrac{\lambda_{ds} - L_s i_{ds}}{L_m} \\ i_{qr} = \dfrac{\lambda_{qs} - L_s i_{qs}}{L_m} \end{cases} \tag{44}$$

$$\begin{cases} \lambda_{dr} = L_m i_{ds} + L_r i_{dr} \\ \lambda_{qr} = L_m i_{qs} + L_r i_{qr} \end{cases} \tag{45}$$

$$\begin{cases} v_{dr} = r_r i_{dr} - (\omega_s - \omega_r)\,\lambda_{qr} \\ v_{qr} = r_r i_{qr} + (\omega_s - \omega_r)\,\lambda_{dr} \end{cases} \tag{46}$$

Then, the active power of the rotor can be computed. The sum of stator and rotor active power should be equal to the total active power from the result of power flow. If not, it needs to adjust the active power of the stator and then compute the variable of the generator using equation (41) - (46) until the error of active power is within a small limit. During the above iterative computation, the power loss of the resistor should be considered.

3) Add the equivalent conductance matrix to the matrix of the system

The equivalent conductance matrix of equation (31) is not changed during the whole transient simulation unless the generator is cut down. The matrix needs to be added to the conductance matrix of the system during initialization, and only the equivalent current of equation (32) is computed during the transient simulation.

V. TRANSIENT SIMULATION PROCESS

The process of electromagnetic transient simulation is shown in Figure 8. It includes the input of power flow data, initialization, solution of the differential equation, solution of the system matrix, etc. The DFIG-based WG is one part of the whole simulation. The computation of DFIG-based WG is described below.

Before the transient simulation, the bus voltage of equation (33) and generator power of DFIG-based WGs is obtained from the result of power flow. The initial value is computed, including the angle related to different axes, the initial value of all variables, and the equivalent conductance matrix, which has been explained in section IV.

The transient simulation begins from 0 to T_{end} with the time-step Δt. For each time step, the computation includes the following 5 steps:

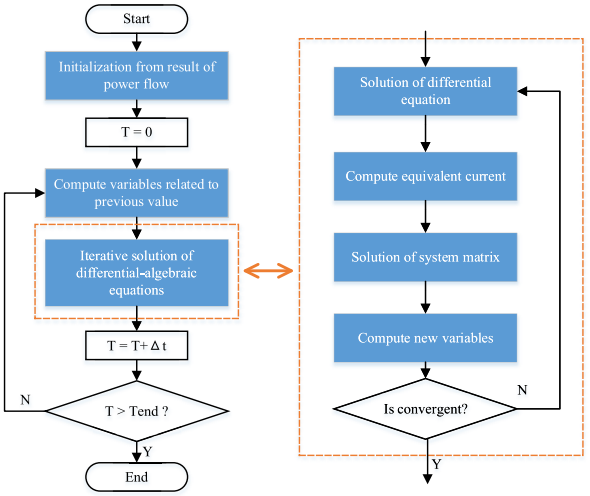

FIGURE 9. The basic flow chart of electromagnetic transient simulation.

1) Compute the variable only related to the previous step

In the computation of differential equation and current source, some parts are only related to the value of the previous step that is usually computed and saved firstly, as shown in equations (21), (22), and (30).

The step is computed only once for each time-step.

2) Solve the differential equation

The differential equation is solved to acquire the discrete value of state variables, and the numerical computation uses the implicit trapezoidal integral method.

For DFIG, equation (5) is solved to get the new value of stator and rotor flux. Using the implicit trapezoidal integral method, equation (47) - (50) can be derived from (5).

$$\begin{cases} \lambda_{ds} = \dfrac{D_{ds} + \dfrac{\Delta t}{2}\omega_s D_{qs}}{1 + \left(\dfrac{\Delta t}{2}\omega_s\right)^2} \\ \lambda_{qs} = \dfrac{-\dfrac{\Delta t}{2}\omega_s D_{ds} + D_{qs}}{1 + \left(\dfrac{\Delta t}{2}\omega_s\right)^2} \end{cases} \tag{47}$$

$$\begin{cases} \lambda_{dr} = \dfrac{D_{dr} + \dfrac{\Delta t}{2}(\omega_s - \omega_r) D_{qr}}{1 + \left(\dfrac{\Delta t}{2}(\omega_s - \omega_r)\right)^2} \\ \lambda_{qr} = \dfrac{-\dfrac{\Delta t}{2}(\omega_s - \omega_r) D_{dr} + D_{qr}}{1 + \left(\dfrac{\Delta t}{2}(\omega_s - \omega_r)\right)^2} \end{cases} \tag{48}$$

$$\begin{cases} D_{ds} = \dfrac{\Delta t}{2}(v_{ds} - r_s i_{ds}) + F_{ds,\Delta t} \\ D_{qs} = \dfrac{\Delta t}{2}\left(v_{qs} - r_s i_{qs}\right) + F_{qs,\Delta t} \end{cases} \tag{49}$$

$$\begin{cases} D_{dr} = \dfrac{\Delta t}{2}\left[v_{dr} - r_r i_{dr}\right] + F_{dr,\Delta t} \\ D_{qr} = \dfrac{\Delta t}{2}\left[v_{qr} - r_r i_{qr}\right] + F_{qr,\Delta t} \end{cases} \tag{50}$$

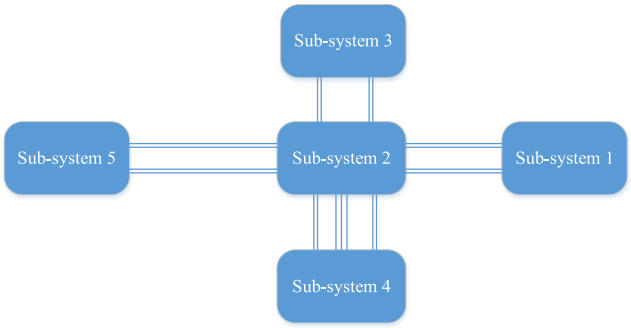

FIGURE 10. The basic structure of the power system.

where $F_{ds,\Delta t}$, $F_{qs,\Delta t}$, $F_{dr,\Delta t}$ and $F_{qr,\Delta t}$ is referred to equation (22) which is computed based on the value of the previous step.

The model of all control systems should be computed in the first step in general.

3) Compute the equivalent current

According to section III, the DFIG-based WG is equivalent to the parallel connection of conductance matrix and current source. The conductance matrix is computed only once in the initialization, and the current source needs to be computed in each time-step using equation (26), in which the newly computed state variables of step 2 are used.

The equivalent current is expressed in the form of three phases and is added to the injection current vector of the power grid.

4) Solve system matrix

The matrix of the power system is usually formed during initialization and is kept constant during the whole transient simulation. After the injection current vector of the power grid is computed, the bus voltage of three phases is solved.

5) Compute new variables

After solving the system matrix, the new bus voltages of three phases are computed, and then some variables need to be computed based on these new bus voltages including the voltage, current of dq-axis, etc., as shown in (51) - (53).

$$\begin{cases} v_{ds} = \frac{2}{3}\left[v_a \cos\theta + v_b \cos\left(\theta - \frac{2\pi}{3}\right) \right. \\ \left. + v_c \cos\left(\theta + \frac{2\pi}{3}\right)\right] \\ v_{qs} = -\frac{2}{3}\left[v_a \sin\theta + v_b \sin\left(\theta - \frac{2\pi}{3}\right) \right. \\ \left. + v_c \sin\left(\theta + \frac{2\pi}{3}\right)\right] \end{cases} \tag{51}$$

$$\begin{cases} i_{ds} = \left(v_{ds} - v_{dseq}\right)/R_{seq} \\ i_{qs} = \left(v_{qs} - v_{qseq}\right)/R_{seq} \end{cases} \tag{52}$$

$$\begin{cases} i_{dr} = \left[\lambda_{ds} - \left(l_m + l_s\right) i_{ds}\right]/l_m \\ i_{qr} = \left[\lambda_{qs} - \left(l_m + l_s\right) i_{qs}\right]/l_m \end{cases} \tag{53}$$

Each time-step is computed iteratively. After the above 5 steps are finished, go back to step 1 to start a new round of computation until the maximum error is within a small limit. The above iterative method can increase accuracy and make the program easier, but the expense is the increased computation. It can also only compute once and does not use the iterative method.

After the computation of each step is finished, the time is changed to the next step and then the subsequent computation is carried out until the time is greater than the end.

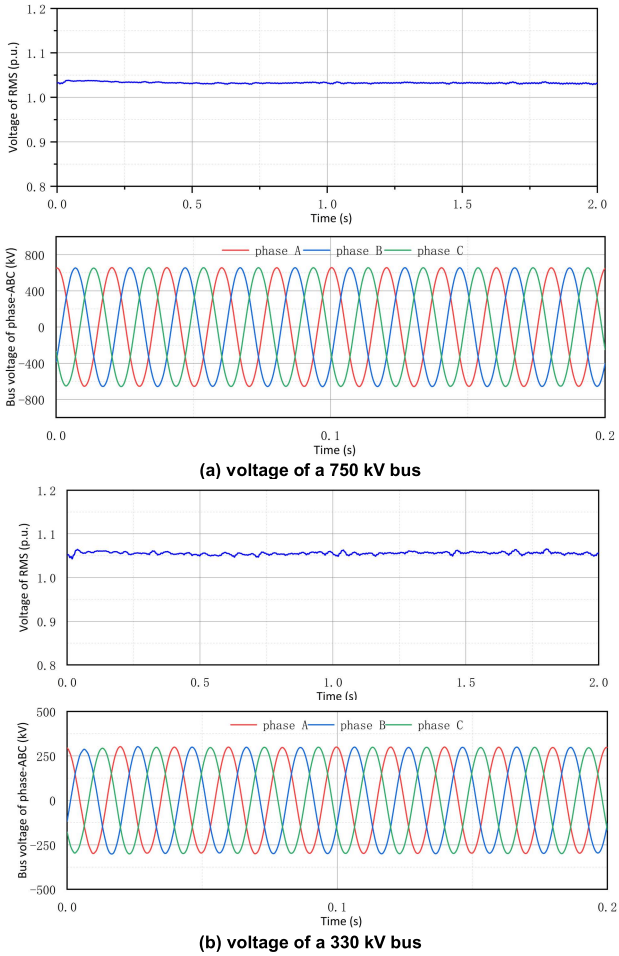

FIGURE 11. The voltage of some buses.

VI. SIMULATION OF REAL POWER SYSTEM

A real power system is simulated and analyzed using the above-proposed simulation method. The basic structure is shown in Figure 10. The power system includes 9889 buses, 569 synchronous generators, and 898 wind farms. It includes five sub-systems connected with 750 kV AC lines. The distribution of wind farms is listed in TABLE 1, in which the total active power of wind farms accounts for 18.7% of the total power of all generators.

Before the transient simulation starts, the power flows are computed and obtained by using the power flow program such as PSD [24] and PSASP [25] which are used widely in China. Based on the result of power flow, the initialization is executed to compute the initial value of all variables. Then the electromagnetic transient simulation begins with a time step of 50 micro-second.

TABLE 1. The number list of wind farms.

Sub-system	Number of wind farms	Active power of wind farms (MW)
1	193	3722.6
2	141	4618.7
3	184	3686.3
4	113	2560.0
5	267	5856.5
total	898	20444.1

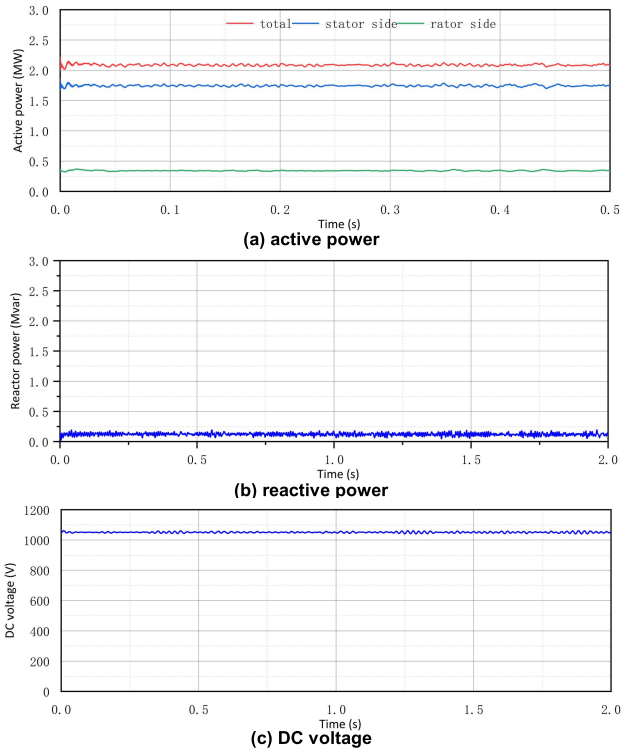

FIGURE 12. Some variables of a DFIG-based WG.

The first simulation is executed without any disturbances, and the simulation time is 2 seconds.

The voltage of some buses is shown in Figure 11 including a 750 kV bus and a 330 kV bus. The left figure is the RMS value and the right figure is the instantaneous value of three-phase *abc*. The curve of instantaneous value only shows the curve from 0 to 0.2 s in order to see it more clearly.

Some variables of a DFIG-based WG are shown in Figure 11 including the active power, reactive power, and DC voltage.

As shown in Figure 11 and Figure 12, the curve is smooth during the whole process, with just a small fluctuation only at the beginning. These results show that the initialization method is successful.

Then, a three-phase short circuit fault is simulated, and some of the results are shown in Figure 13, which include the voltage of two buses and the power of two DFIG-based WGs in different wind farms. The electromechanical transient simulation is usually used for large-scale power systems, and should have comparability with the result. Thus, the result is also shown in Figure 13, which is simulated by PSD software.

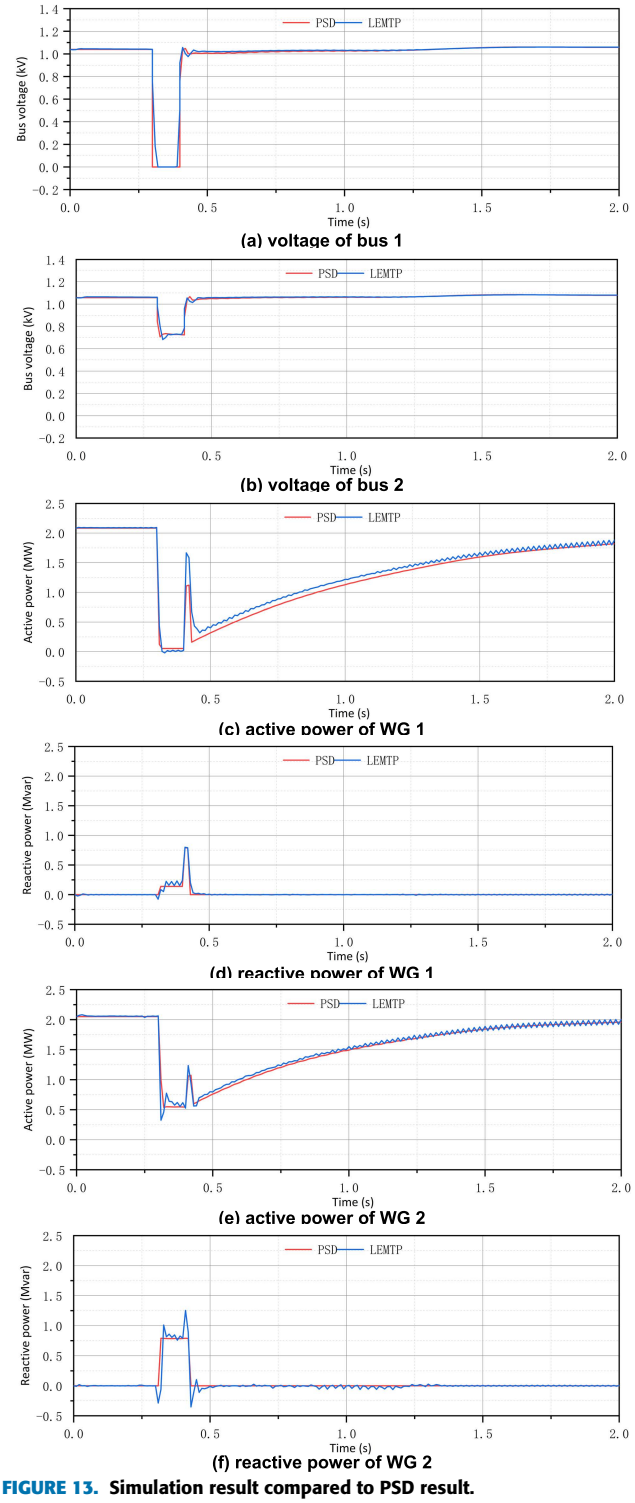

FIGURE 13. Simulation result compared to PSD result.

From the result of Figure 13, all the results are reasonable and consistent with the curve of electromechanical transient simulation according to the theoretical analysis. Therefore, the whole simulation process proves correct and smooth.

The electromagnetic transient model of DFIG-based WG is similar to the model of the traditional model of electromagnetic software, so it can be verified easily. But for

large scale power system, it is almost impossible to use the current electromagnetic transient simulation software, and only the electromechanical transient simulation is usually used. So, the result of electromagnetic transient simulation can only be compared with the existing electromechanical transient simulation software. However, there always exist some differences between electromagnetic and electromechanical transient simulation. The verification should consider the correctness of theory and consistency of trend. The specific comparison methods may need in-depth study in the future.

VII. CONCLUSION

In order to enhance the capability of the simulation tools in the face of increasing deployment of RESs, a novel electromagnetic simulation method for large-scale AC power systems with high penetrations of DFIG-based wind farms is proposed and evaluated. The paper elaborates the method from the following aspects: modeling, interface, initialization, and simulation process.

1) The modeling mainly considers the external characteristics related to AC power system and ignores the detailed switching processes. So, the convertor of DFIG-based WG is simplified to a controlled voltage source with some limits. The model can greatly improve simulation efficiency.

2) The interface, which is equivalent to the NORTON circuit, joins the DFIG-based WG and the AC power grid. The interfaces of the stator of the generator and the converter of the grid-side need to be processed separately.

3) The initialization, by taking a reference from the electromechanic transient simulation, is based on the result of power flow. The first step of initialization is to establish the relationships among the instantaneous value, RMS value, and *dq*-axis value. Then the initial values of all variables can be computed.

4) The transient simulation process is similar to the electromechanic transient simulation program. After reading data from the power flow result, all the variables are initialized, and then the transient simulation begins. The simulation of every time step includes solving differential equations, computing injected currents, solving network equations, and computing variables.

Simulation results for a real power system with 9889 buses and 898 wind farms with the above method show that the simulation can start smoothly and has great accuracy. The study establishes the foundation and provides reference for developing powerful simulation tools that can address the electromagnetic transient processes of future power systems. On this foundation, there are still many problems to be explored, such as the simulation method of HVDC [26]–[28], multi-rate simulation [29]–[31], verification method of correctness, parallel computation, etc.

REFERENCES

[1] *Energy and Power Analysis Annual Report Series—China 2020 New Energy Generation Analysis Report*, State Grid Energy Inst. Co. Ltd., China Electr. Power Press, Beijing, China, 2020, pp. 6–16.

[2] B. Huang, Y. Zhang, and C. Wang, "New energy development and issues in China during the 14th five-year plan," *Eletr. Power*, vol. 53, no. 1, pp. 1–9, Jan. 2020.

[3] Z. Tang, Y. Yang, and F. Blaabjerg, "Power electronics: The enabling technology for renewable energy integration," *Proc. CSEE*, vol. 8, no. 1, pp. 39–52, Jan. 2022, doi: 10.17775/CSEEJPES.2021.02850.

[4] Z. Zhuo, N. Zhang, X. Xie, Z. Li, and C. Kang, "Key technologies and developing challenges of power system with high proportion of renewable energy," *Autom. Electr. Power Syst.*, vol. 45, no. 9, pp. 171–191, May 2021.

[5] M. Tsili and S. Papathanassiou, "A review of grid code technical requirements for wind farms," *IET Renew. Power Gener.*, vol. 3, no. 3, pp. 308–332, Mar. 2009, doi: 10.1049/iet-rpg.2008.0070.

[6] D. Peng, H. Tao, Z. Yiying, W. Weiwei, and L. Chong, "The impact of LVRT characteristic on the stability of northwest China grid with large scale wind power," in *Proc. 2nd IET Renew. Power Gener. Conf. (RPG)*, 2013, pp. 1–6, doi: 10.1049/cp.2013.1752.

[7] P. Sun, J. Yao, S. Huang, Y. Luo, and X. Fang, "Dynamic stability analysis and improved control strategy of DFIG system during LVRT," in *Proc. IEEE 5th Conf. Energy Internet Energy Syst. Integr. (EI)*, Oct. 2021, pp. 354–358, doi: 10.1109/EI252483.2021.9712938.

[8] W. Du, C. Chen, and H. Wang, "Subsynchronous interactions induced by DFIGs in power systems without series compensated lines," *IEEE Trans. Sustain. Energy*, vol. 9, no. 3, pp. 1275–1284, Jul. 2018, doi: 10.1109/TSTE.2017.2781289.

[9] Y. Wang, Q. Wu, and S. Kang, "Sub-synchronous interaction analysis between DFIG based wind farm and series compensated network," in *Proc. IEEE PES Asia–Pacific Power Energy Eng. Conf. (APPEEC)*, Oct. 2016, pp. 359–363, doi: 10.1109/APPEEC.2016.7779527.

[10] (Nov. 21, 2018). Manitoba Hydro International Ltd. *Type 3 Wind Turbine Generators (WTG), PSCAD v4.6*. [Online]. Available: https://www.pscad.com/knowl edge-base/article/496.

[11] (Jul. 1, 2021). Opal-RT Technologies. *Microgrid Real-Time Simulation*. [Online]. Available: https://www.opal-rt.com/resource-center/document/?resource=Mkt_0027277

[12] H. W. Dommel, *Electromagnetic Transients Program: Reference Manual: (EMTP Theory Book)*, Portland, OR, USA: Bonneville Power Administration, 1986, pp. 1–9.

[13] P. Kundur, *Power System Stability and Control*. New York, NY, USA: McGraw-Hill, 1994, pp. 18–27.

[14] R. Pena, J. C. Clare, and G. M. Asher, "Doubly fed induction generator using back-to-back PWM converters and its application to variable-speed wind-energy generation," in *Proc. IEE Proc.-Electr. Power Appl.*, vol. 143, no. 3, pp. 231–241, May 1996, doi: 10.1049/ip-epa:19960288.

[15] R. Pena, J. C. Clare, and G. M. Asher, "A doubly fed induction generator using back-to-back PWM converters supplying an isolated load from a variable speed wind turbine," *IEE Proc.-Electr. Power Appl.*, vol. 143, no. 5, pp. 380–387, Sep. 1996, doi: 10.1049/ip-epa:19960454.

[16] L. Xu and Y. Wang, "Dynamic modeling and control of DFIG-based wind turbines under unbalanced network conditions," *IEEE Trans. Power Syst.*, vol. 22, no. 1, pp. 314–323, Feb. 2007, doi: 10.1109/TPWRS.2006.889113.

[17] M. Castilla, J. Miret, J. Matas, A. Borrell, and L. G. de Vicuña, "Direct rotor current-mode control improves the transient response of doubly fed induction generator-based wind turbines," *IEEE Trans. Energy Convers.*, vol. 25, no. 3, pp. 722–731, Sep. 2010, doi: 10.1109/TEC.2010.2052105.

[18] H. Mirnezhad, M. H. Ravanji, and M. Parniani, "Improved generic model of variable speed wind turbines for dynamic studies," *IEEE Trans. Sustain. Energy*, vol. 11, no. 4, pp. 2162–2173, Oct. 2020, doi: 10.1109/TSTE.2019.2952144.

[19] P. Pourbeik, J. J. Sanchez-Gasca, J. Senthil, J. D. Weber, P. S. Zadehkhost, Y. Kazachkov, S. Tacke, J. Wen, and A. Ellis, "Generic dynamic models for modeling wind power plants and other renewable technologies in large-scale power system studies," *IEEE Trans. Energy Convers.*, vol. 32, no. 3, pp. 1108–1116, Sep. 2017, doi: 10.1109/TEC.2016.2639050.

[20] M. Kheshti, X. Kang, G. Song, and Z. Jiao, "Modeling and fault analysis of doubly fed induction generators for Gansu wind farm application," *Can. J. Elect. Comput. Eng.*, vol. 38, no. 1, pp. 52–64, 2015, doi: 10.1109/CJECE.2014.2359682.

[21] D. Xie, Z. Xu, L. Yang, J. Ostergaard, Y. Xue, and K. Wong, "A comprehensive LVRT control strategy for DFIG wind turbines with enhanced reactive power support," *IEEE Trans. Power Syst.*, vol. 28, no. 3, pp. 3302–3310, Aug. 2013, doi: 10.1109/TPWRS.2013.2240707.

[22] F. L. Alvarado, R. H. Lasseter, and J. J. Sanchez, "Testing of trapezoidal integration with damping for the solution of power transient problems," *IEEE Trans. Power Appar. Syst.*, vol. PAS-102, no. 12, pp. 3783–3790, Dec. 1983, doi: 10.1109/TPAS.1983.317872.
[23] H. W. Dommel and N. Sato, "Fast transient stability solutions," *IEEE Trans. Power App. Syst.*, vol. PAS-91, no. 4, pp. 1643–1650, Jul. 1972, doi: 10.1109/TPAS.1972.293341.
[24] *PSD-BPA Electro-Mechanic Transient Simulation Program User Manual*, China Electr. Power Res. Inst., Beijing, China, 2021, pp. 1–9.
[25] *Power System Analysis Solver Package User Manual*, China Electr. Power Res. Inst., Beijing, China, 2021, pp. 1–5.
[26] W. Wang, F. Dou, J. Cheng, X. Yu, M. Yang, and Q. Huang, "Modeling and simulation of ±800 kV HVDC electromagnetic transients," in *Proc. Asia Energy Electr. Eng. Symp. (AEEES)*, May 2020, pp. 465–470, doi: 10.1109/AEEES48850.2020.9121384.
[27] H. Saad, J. Peralta, S. Dennetiere, J. Mahseredjian, J. Jatskevich, J. A. Martinez, and A. Davoudi, "Dynamic averaged and simplified models for MMC-based HVDC transmission systems," *IEEE Trans. Power Deliv.*, vol. 28, no. 3, pp. 1723–1730, Jul. 2013, doi: 10.1109/TPWRD.2013.2251912.
[28] S. Gao, H. Zhu, B. Zhang, and G. Song, "Modeling and simulation analysis of hybrid bipolar HVDC system based on LCC-HVDC and VSC-HVDC," in *Proc. IEEE 3rd Adv. Inf. Technol., Electron. Autom. Control Conf. (IAEAC)*, Oct. 2018, pp. 1448–1452, doi: 10.1109/IAEAC.2018.8577863.
[29] J. G. Pearce, R. E. Crosbie, J. J. Zenor, R. Bednar, D. Word, and N. G. Hingorani, "Developments and applications of multi-rate simulation," in *Proc. 11th Int. Conf. Comput. Model. Simul.*, 2009, pp. 129–133, doi: 10.1109/UKSIM.2009.23.
[30] S. D. Pekarek, O. Wasynczuk, E. A. Walters, J. V. Jatskevich, C. E. Lucas, N. Wu, and P. T. Lamm, "An efficient multirate Simulation technique for power-electronic-based systems," *IEEE Trans. Power Syst.*, vol. 19, no. 1, pp. 399–409, Feb. 2004, doi: 10.1109/TPWRS.2003.821452.
[31] M. L. Crow and J. G. Chen, "The multirate method for simulation of power system dynamics," *IEEE Trans. Power Syst.*, vol. 9, no. 3, pp. 1684–1690, Aug. 1994, doi: 10.1109/59.336087.
[32] H. Ouquelle, L.-A. Dessaint, and S. Casoria, "An average value model-based design of a deadbeat controller for VSC-HVDC transmission link," in *Proc. IEEE Power Energy Soc. Gen. Meeting*, Jul. 2009, pp. 1–6, doi: 10.1109/PES.2009.5275748.
[33] J. Peralta, H. Saad, and S. Dennetiere, "Dynamic performance of average-value models for multi-terminal VSC-HVDC systems," in *Proc. IEEE Power Energy Soc. Gen. Meeting*, Jul. 2012, pp. 1–8, doi: 10.1109/PESGM.2012.6345610.

YIFENG DONG was born in Hunan, China, in 1985. He received the B.S. and M.S. degrees in electrical engineering from Tianjin University, Tianjin, China, in 2007 and 2009, respectively. He is currently pursuing the Ph.D. degree in electrical engineering with the Huazhong University of Science and Technology (HUST), Wuhan, China.

His research interests include power system simulation, power system planning, and electricity market.

JIANBO GUO (Senior Member, IEEE) received the B.S. degree from the Huazhong University of Science and Technology (HUST), Wuhan, China, in 1982, and the M.S. degree from the China Electric Power Research Institute, Beijing, China, in 1984.

Since 2013, he has been an Elected Academician with the Chinese Academy of Engineering, Beijing. He is currently the Honorary President of China Electric Power Research Institute and the Deputy Chief Engineer of State Grid Corporation of China. He has long engaged in power system analysis and control.

SHIHONG MIAO (Member, IEEE) was born in Hubei, China, in 1963. He received the M.S. and Ph.D. degrees in electrical engineering from the Huazhong University of Science and Technology (HUST), Wuhan, China, in 1996 and 2003, respectively.

He is currently a Professor with the School of Electrical and Electronic Engineering, HUST. His research interests include power system protective relaying and control, renewable energy technology, novel distribution network and micro-grid technology, and compressed air energy storage (CAES) technology.

JUNXIAN HOU received the B.S. degree in electrical engineering from Shanghai Jiaotong University, Shanghai, China, in 1999, the M.S. degree from the China Electric Power Research Institute, Beijing, China, in 2002, and the Ph.D. degree from North China Electric Power University (NCEPU), Beijing, in 2016.

His research interests include power system simulation and power system operation.

JI HAN (Student Member, IEEE) was born in Liaoning, China, in 1993. He received the B.S. degree in electrical engineering from the Huazhong University of Science and Technology (HUST), Wuhan, China, in 2016, where he is currently pursuing the Ph.D. degree.

His research interests include application of machine learning in power systems, renewable energy technology, and fault diagnosis of power systems.

SHICONG MA received the B.S. and Ph.D. degrees from Shandong University, in 2002 and 2008, respectively.

He visited Alstom Power Grid, U.K., in 2010. He worked as a Postdoctoral Researcher with the China Electric Power Research Institute, from 2011 to 2013. He is currently a Senior Engineer with the Power System Department, China Electric Power Research Institute. His current interests include the areas of power system security and stability analysis, artificial intelligence in power system applications, complex networks, and autonomous power systems.

TIEZHU WANG received the B.S. degree in electrical engineering from Tsinghua University, Beijing, China, in 2012, and the M.S. degree in electrical engineering from the China Electric Power Research Institute, Beijing, in 2015, where he is currently pursuing the Ph.D. degree with the Power System Department.

His current research interests include LCC-HVDC, VSC-HVDC, power system simulation, and stability analysis for the power systems with high penetrations of power electronics.